# Influence of Excited-State-Energy Upconversion on Pulse Shape in Quasi-Continuous-Wave Diode-Pumped Er:$LiYF_4$ Lasers

Niklaus Ursus Wetter, Alessandro Melo Deana, Izilda Marcia Ranieri, Laércio Gomes, and Sonia Licia Baldochi

***Abstract*—In this paper, we demonstrate the temporal dependency of an Er:$LiYF_4$ laser on the upper laser level energy transfer upconversion. By spectroscopic measurements and numerical simulations, we calculate a value for this upconversion of $9 \times 10^{-17}$ $cm^3/s$. We also report a 60% higher average output power for short-pulse duration, which is complementary to some earlier findings.**

***Index Terms*—Diode-pumped lasers, infrared lasers, lasers for biomedical applications, rare earth lasers.**

## I. Introduction

In RECENT years, there has been an enormous interest in obtaining and optimizing lasers in the 3 $\mu$m region because of the strong absorption due to the OH vibration of water vapor, liquid water [1], and consequently, biological tissue [2]. Therefore, this wavelength may be used for light detection and ranging (LIDAR) [1] measurements of atmospheric humidity and laser surgery. For laser surgery, a small laser system is desirable with high rep rate and pulses of hundreds of microseconds [2]. The erbium laser may be efficiently diode pumped at 970 nm [3].

Depending on the host material, the $^4I_{11/2} \rightarrow ^4 I_{13/2}$ Erbium transition emits between 2.7 and 2.94 $\mu$m. Several energy transfer processes occur simultaneously in the Er:$LiYF_4$ (Er:YLF) crystal during the laser operation, some of which are difficult to measure, including the key process $W_{22}$. This energy transfer upconversion (ETU) process is responsible for depopulating the upper laser level, therefore decreasing the output power. The presented results show that it is this process, which is predominant in shaping the temporal behavior of the lasers' output pulse in quasi-continuous-wave (qCW) operation.

The energy level diagram of Fig. 1 shows the most significant processes involved in the laser operation. Although there are many mechanisms operating simultaneously, the lasing behavior can be qualitatively explained by four main processes [4]:

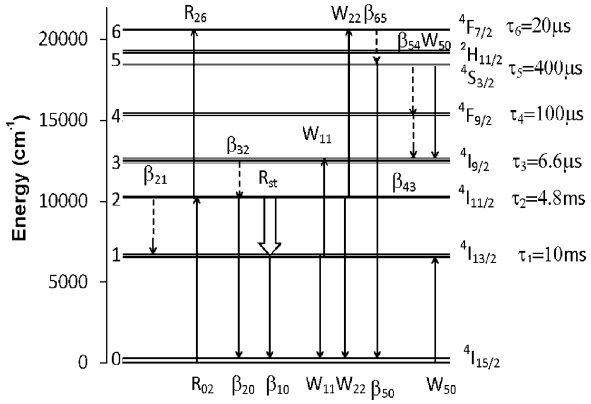


Fig. 1. Energy level scheme of Er:YLF showing the relevant processes involved in the laser operation. $W_{11}$ and $W_{22}$ are ETUs, $W_{50}$ is a cross-relaxation, $R_{\rm st}$ the stimulated emission, and $R_{26}$ is the ESA. The relative rates of these processes can be found in Table I.

the ground-state absorption (GSA) of the 973 nm pump wavelength directly populates the upper laser level $^4I_{11/2}$. Once this level populates, there are two main competing mechanisms depopulating it: the stimulated emission, which is proportional to the population of this level, and the energy transfer $W_{22}$, which is proportional to the square of this population. The $W_{22}$ ETU introduces a loss in the laser channel that grows at a faster rate than the stimulated emission. It has been shown that the $W_{22}$ is much more significant than the also competing excited state absorption (ESA) [4]. Both $W_{22}$ and ESA eventually occupy the $^4S_{3/2}$ energy level after nonradiative decay, from where the cross-relaxation $W_{50}$ redistributes the energy to the upper and lower laser level. The stimulated emission $R_{\rm st}$ populates the $^4I_{13/2}$ lower laser level and a second ETU, $W_{11}$, redistributes its energy to the ground level and also back to the upper laser level. This second ETU is the main responsible mechanism for CW operation in Er:YLF. Due to the long $^4I_{13/2}$ lower laser level life time, this laser would be self-terminating if the $W_{11}$ process did not exist. Due to the $W_{11}$ ETU this laser operates CW by directly pumping into the lower laser level [5].

## II. Experimental Setup

The main resonator is pumped by a fiber-bundle-coupled diode array (Opto power model BF-NSI-ENG) and delivers 21.5 W of output power at 975 nm after the focusing optics. The diode was mounted on a thermoelectric cooler that was temperature stabilized to within $\pm 0.1\,^\circ$C, using a temperature controller and a feedback loop. The focusing optics delivered a

Manuscript received March 17, 2009; revised May 26, 2009. Current version published December 04, 2009.

N. U. Wetter, I. M. Ranieri, L. Gomes, and S. L. Baldochi are with the Instituto de Pesquisas Energéticas e Nucleares, Centro de Lasers e Aplicações, CNEN-IPEN/SP, 2242 São Paulo, Brazil (e-mail: nuwetter@ipen.br; iranieri@ipen.br; lgomes@ipen.br; baldochi@ipen.br).

A. M. Deana is with the Instituto de Pesquisas Energéticas e Nucleares, Centro de Lasers e Aplicações, CNEN-IPEN/SP, 2242 São Paulo, Brazil, and also with MedCompany, São Paulo, Brazil (e-mail: amdeana@gmail.com).

Color versions of one or more of the figures in this paper are available online at http://ieeexplore.ieee.org.

Digital Object Identifier 10.1109/JQE.2009.2028305

TABLE I
PARAMETERS USED FOR THE NUMERICAL SIMULATIONS

| Parameter | Value |
|---|---|
| fluorescence lifetime $^4I_{13/2}$ ($\tau_1$) | 10x10$^{-3}$ s [8] |
| fluorescence lifetime $^4I_{11/2}$ ($\tau_2$) | 4.8x10$^{-3}$ s [9] |
| fluorescence lifetime $^4I_{9/2}$ ($\tau_3$) | 6.6x10$^{-6}$ s [9] |
| fluorescence lifetime $^4F_{9/2}$ ($\tau_4$) | 100x10$^{-6}$ s [8] |
| fluorescence lifetime $^4H_{11/2}$ & $^2S_{3/2}$ ($\tau_5$) | 400x10$^{-6}$ s [8] |
| fluorescence lifetime $^4F_{7/2}$ ($\tau_6$) | 20x10$^{-6}$ s [4] |
| Laser emission cross section $\sigma_{21}$ | 3x10$^{-20}$ cm$^2$ [4] |
| ground state absorption $\sigma_{02}$ | 0.6x10$^{-20}$ cm$^2$ [10] |
| excited state absorption $\sigma_{26}$ | 0.8x10$^{-20}$ cm$^2$ [10] |
| upper laser level Boltzmann occupation factor $b_2$ | 2x10$^{-1}$ |
| lower laser level Boltzmann occupation factor $b_1$ | 1.13x10$^{-1}$ |
| branching ratio $\beta_{10}$ : $^4I_{13/2} \rightarrow {}^4I_{15/2}$ | 1 [4] |
| branching ratio $\beta_{20}$ : $^4I_{11/2} \rightarrow {}^4I_{15/2}$ | 0.613 [4] |
| branching ratio $\beta_{30}$ : $^4I_{9/2} \rightarrow {}^4I_{15/2}$ | 0.001 [4] |
| branching ratio $\beta_{40}$ : $^4F_{9/2} \rightarrow {}^4I_{15/2}$ | 0.087 [4] |
| branching ratio $\beta_{51}$ : $^4H_{11/2}$ & $^2S_{3/2} \rightarrow {}^4I_{13/2}$ | 0.488 [4] |
| branching ratio $\beta_{60}$ : $^4F_{7/2} \rightarrow {}^4I_{15/2}$ | 0.051 [4] |
| branching ratio $\beta_{21}$ : $^4I_{11/2} \rightarrow {}^4I_{13/2}$ | 0.387 [4] |
| branching ratio $\beta_{31}$ : $^4I_{9/2} \rightarrow {}^4I_{13/2}$ | 0 [4] |
| branching ratio $\beta_{41}$ : $^4F_{9/2} \rightarrow {}^4I_{13/2}$ | 0.004 [4] |
| branching ratio $\beta_{51}$ : $^4H_{11/2}$ & $^2S_{3/2} \rightarrow {}^4I_{13/2}$ | 0.179 [4] |
| branching ratio $\beta_{61}$ : $^4F_{7/2} \rightarrow {}^4I_{13/2}$ | 0.004 [4] |
| branching ratio $\beta_{32}$ : $^4I_{9/2} \rightarrow {}^4I_{11/2}$ | 0.999 [4] |
| branching ratio $\beta_{42}$ : $^4F_{9/2} \rightarrow {}^4I_{11/2}$ | 0.006 [4] |
| branching ratio $\beta_{52}$ : $^4H_{11/2}$ & $^2S_{3/2} \rightarrow {}^4I_{11/2}$ | 0.015 [4] |
| branching ratio $\beta_{62}$ : $^4F_{7/2} \rightarrow {}^4I_{11/2}$ | 0.002 [4] |
| branching ratio $\beta_{43}$ : $^4F_{9/2} \rightarrow {}^4I_{9/2}$ | 0.903 [4] |
| branching ratio $\beta_{53}$ : $^4H_{11/2}$ & $^2S_{3/2} \rightarrow {}^4I_{9/2}$ | 0.012 [4] |
| branching ratio $\beta_{63}$ : $^4F_{7/2} \rightarrow {}^4I_{9/2}$ | 0.002 [4] |
| branching ratio $\beta_{54}$ : $^4H_{11/2}$ & $^2S_{3/2} \rightarrow {}^4F_{9/2}$ | 0.306 [4] |
| branching ratio $\beta_{64}$ : $^4F_{7/2} \rightarrow {}^4F_{9/2}$ | 0 [4] |
| branching ratio $\beta_{65}$ : $^4F_{7/2} \rightarrow {}^4H_{11/2}$ & $^2S_{3/2}$ | 0.941 [4] |
| nominal pump power $P_{IN}$ | 21.5 W |
| pump delivery efficiency $\eta_T$ | 0.95 |
| mode fill efficiency $\eta_B$ | 0.77 |
| cavity transmission given by $T = 1\text{-}loss$ | 0.961 |
| output mirror reflectivity $R$ | 0.986 |
| energy transfer upconversion from $^4I_{13/2}$ : $W_{11}$ | 3x10$^{-17}$ cm$^3$/s [9] |
| cross relaxation from $^4H_{11/2}$ & $^2S_{3/2}$ : $W_{50}$ | 2x10$^{-16}$ cm$^3$/s [11] |
| energy transfer upconversion from $^4I_{11/2}$ : $W_{22}$ | 1.8x10$^{-17}$ cm$^3$/s [9] |
| erbium concentration $N_0$ | 2.1x10$^{21}$ cm$^{-3}$ |
| crystal length $L_{CR}$ | 4.5 mm |
| cavity length $L_{CAV}$ | 2 cm |
| laser pump wavelength $\lambda_P$ | 973 nm |
| Laser emission wavelength $\lambda_L$ | 2.8 μm |
| degeneracy of upper and lower laser levels $d_{UP}$, $d_{LOW}$ | 2 |
| laser mode cross section $A_{mode}$ | 0.138 mm$^2$ |
| $^4I_{11/2} \rightarrow {}^4I_{13/2}$ radiatively emitted decay rate $f_{DR}$ | 0.29 [4] |

high intensity circular beam with focus dimensions of 232 $\mu$m radius and beam quality of $M^2 = 159$, which was focused at the surface of the crystal. Pump beam parameters were measured with a CCD coupled to a PC and dedicated software (Newport, model. LBP-4-USB) and also using the knife edge method to measure the $M^2$ value [6].

The rare earth fluorides were prepared from pure oxide powders (Aldrich, 99.99%) by hydrofluorination at high temperature in HF + Ar atmosphere. The LiF–$LnF_3$ (Ln = Y and Er) mixture was melted using an open platinum boat in the same atmosphere, with a composition of 1.02 LiF:1 $LnF_3$. The LiF powder (Alpha-Johnson Matthey, 99.9%) was zone-refined before it was added to the mixture. The crystal was grown by the Czochralski method using automatic diameter control under a Ar + $CF_4$ atmosphere, with growth rate of 1.30 mm/h and rotation rate of 10 rpm for the ⟨100⟩-oriented boule.

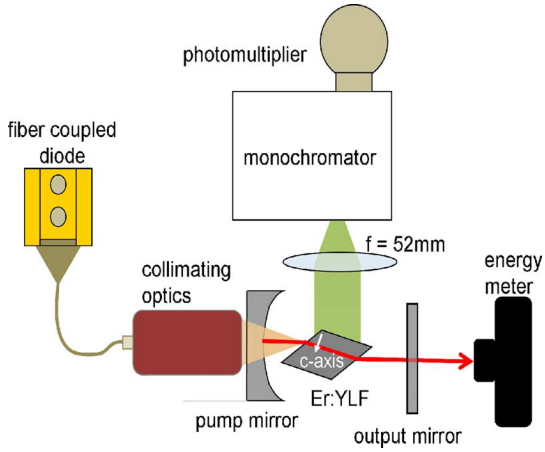


Fig. 2. Schematic layout of the end-pumped Er:YLF resonator with detection apparatus.

A schematic of the laser setup is shown in Fig. 2. The cavity length was 2 cm and the crystal with 15 mol% ($2.1 \times 10^{21}$ cm$^{-3}$) erbium concentration was a-cut at Brewster angle for pi-emission (polarization along the crystal $c$-axis). The 4.5-mm-long crystal was placed inside a planoconcave, end-pumped resonator, based on a concave pump mirror with 10 cm radius of curvature, highly reflective (>99.3%) at 2.8 $\mu$m and with high transmission at 973 nm. The flat output coupler, made of $CaF_2$, had 1.4% transmission at 2.8 $\mu$m [7]. To avoid thermal fracture, the duty cycle was kept below 5% and the pump pulse duration was varied from 100 $\mu$s to several milliseconds. The temporal behavior of the output pulse was analyzed with a thermoelectrically cooled, fast rise time (<2 ns), InAs detector (Virgo System InAs-PVI-2TE), coupled to a 20 MHz preamplifier (Virgo VPDC-201). The pulses were recorded with digital storage oscilloscope (Tektronix TDS 360). Care was taken to attenuate the pulses in order to avoid saturation effects of the detector. The beam energy was measured using an energy meter (Ophir NOVA 2 with PE50-V2 for long pulse and a PE9-V2 for pulses with short duration).

Spontaneous emission at 550 nm emitted from the $^2S_{3/2}$ energy level was monitored at 90° using a custom monochromator and a photomultiplier (Newport, model 70107).

## III. RATE EQUATIONS

A numerical, time-resolved simulation was used that included all energy levels of Fig. 1 up to the $^4F_{7/2}$ level. The system of seven differential, nonlinear equations was solved using a fourth-order Runge–Kutta algorithm. The parameters used for the numerical simulation are shown in Table I.

The rate equations for the population densities $N_i$ (the energy levels are labeled as in Fig. 1) and the photon density $\phi$ are given by [4]

$$\frac{dn_0}{dt} = -\sum_{i=1}^{6} R_{0i}N_0 + \sum_{i=1}^{6} \frac{\beta_{i0}}{\tau_i}N_i - W_{50}(N_5N_0 - N_3N_1) + W_{11}({N_1}^2 - N_3N_0) + W_{22}({N_2}^2 - N_6N_0) \quad (1)$$

$$\frac{dn_1}{dt} = \sum_{i=2}^{6} \frac{\beta_{i1}}{\tau_i} N_i - \frac{N_1}{\tau_1} + W_{50}(N_5 N_0 - N_3 N_1) - 2W_{11}({N_1}^2 - N_3 N_0) + R_{\mathrm{SE}} \quad (2)$$

$$\frac{dn_2}{dt} = R_{02} N_0 - R_{26} N_2 + \sum_{i=3}^{6} \frac{\beta_{i2}}{\tau_i} N_i - \frac{N_2}{\tau_2} - 2W_{22}({N_2}^2 - N_6 N_0) - R_{\mathrm{SE}} \quad (3)$$

$$\frac{dn_3}{dt} = \sum_{i=4}^{6} \frac{\beta_{i3}}{\tau_i} N_i - \frac{N_3}{\tau_3} + W_{50}(N_5 N_0 - N_3 N_1) + W_{11}({N_1}^2 - N_3 N_0) \quad (4)$$

$$\frac{dN_4}{dt} = \sum_{i=5}^{6} \frac{\beta_{i4}}{\tau_i} N_i - \frac{N_4}{\tau_4} \quad (5)$$

$$\frac{dN_5}{dt} = \frac{\beta_{65}}{\tau_6} N_6 - \frac{N_5}{\tau_5} - W_{50}(N_5 N_0 - N_3 N_1) \quad (6)$$

$$\frac{dN_6}{dt} = R_{26} N_2 - \frac{N_6}{\tau_6} + W_{22}(N_2^2 - N_6 N_0) \quad (7)$$

$$\frac{d\phi}{dt} = \frac{L_{\mathrm{CR}}}{R_{\mathrm{CAV}}} \left( R_{\mathrm{SE}} + f_G f_{\mathrm{DR}} \frac{N_2}{\tau_2} \beta_{26} \right) + \frac{\ln(RT) c\phi}{2L_{\mathrm{CAV}}}. \quad (8)$$

Here, $c$ is the speed of light and the stimulated emission rate $R_{\mathrm{SE}}$ as a function of the photon density is given by

$$R_{\mathrm{SE}} = \left( b_2 N_2 - \frac{d_{\mathrm{UP}}}{d_{\mathrm{LOW}}} b_1 N_1 \right) \sigma_{21} c\phi. \quad (9)$$

The energy levels are labeled, as shown in Fig. 1. Since the $^4\mathrm{H}_{11/2}$ and $^2\mathrm{S}_{3/2}$ levels are thermally coupled, they are treated as one combined level 5. The geometrical fraction of the spontaneous emission coupled to the laser mode is [14] given by

$$f_G = \frac{A_{\mathrm{mode}}}{4\pi L_{\mathrm{CAV}}^2}. \quad (10)$$

The pump rates $R_{ij}$ are given by

$$R_{ij} = \frac{\sigma_{ij}}{\alpha} \frac{\eta_B \eta_T \lambda_p}{hcL_{cr} A_{\mathrm{mode}}} (1 - \exp(-\alpha L_{cr})) P_{\mathrm{in}} \quad (11)$$

$$\alpha = \sum_{i=0}^{6} \sum_{j=i+1}^{6} \sigma_{ij} N_i. \quad (12)$$

The output power of the laser is calculated by

$$P_{\mathrm{OUT}} = \frac{1-R}{2} c\phi \frac{hc}{\lambda_L} A_{\mathrm{mode}}. \quad (13)$$

## IV. Laser Results and Simulations

A typical measurement of the output power as a function of time at a pump power of 21.5 W can be found in Fig. 3(a), where we have plotted the average of 64 measurements in order to decrease the amplitude of the oscillation relaxations. It can be observed that there is a clear maximum in output power at the beginning of the laser operation accompanied by strong oscillation relaxations, followed by a second, distinctly different phase with less relaxation oscillations and a more stable laser operation of almost constant average output power.

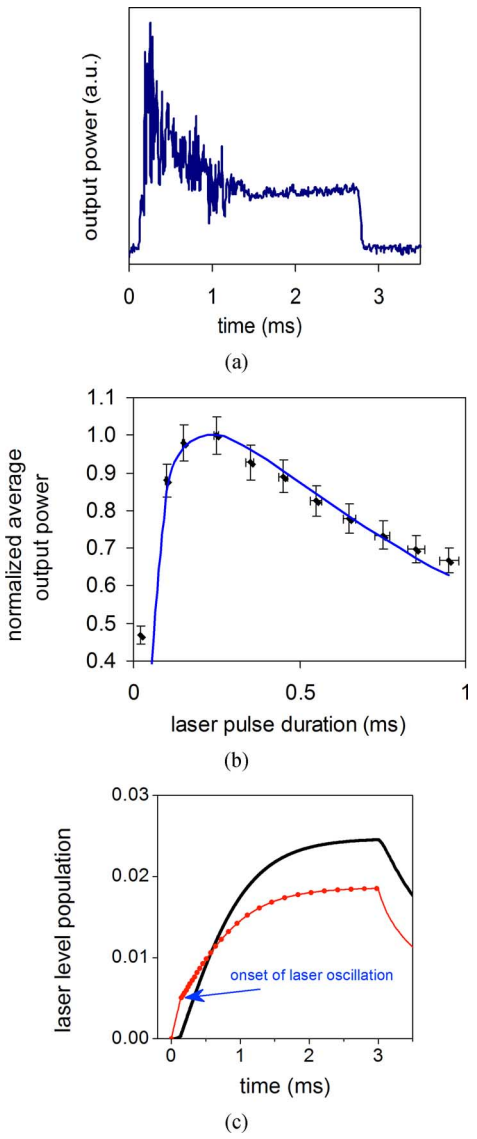


Fig. 3. (a) Oscilloscope trace of the Er:YLF laser pulse (averaged over 64 pulses). (b) Normalized average output power as a function of the qCW pulse duration with numerical fit using $W_{22}$ of $9 \times 10^{-17}$ cm$^3$/s. (c) Simulation of total fraction of upper (dotted line) and lower (straight line) laser level occupation.

In Fig. 3(a), it can be observed that the highest output power is achieved at the beginning of the pulse. To show that this effect is real and does not depend on the pulse acquisition system, we measured the pulse energy as a function of the qCW pulse duration and calculated the average output power during the pulse (see Fig. 3(b); shown are normalized values). This was done for the period of strong oscillation relaxation, which extends to 1 ms after pulse initiation. The delay between the beginning of the pump pulse and the beginning of the laser pulse was 90 $\mu$s. As can be seen in Fig. 3(b), the highest average output power was achieved for a pulse duration of 250 $\mu$s. Its average output power is approximately 60% higher than for long pulses

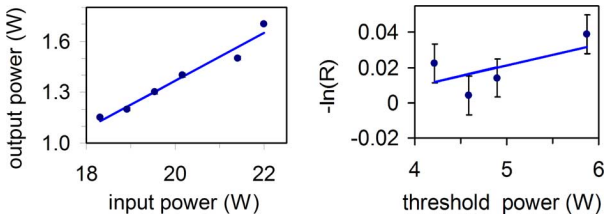


Fig. 4. (Left) Output power as a function of input power for 250-$\mu$s-long pump pulses. (Right) Findlay–Clay analysis of the laser losses.

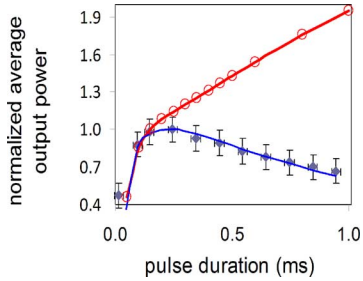


Fig. 5. (Lower curve) Experimentally obtained and normalized average output power as a function of pulse duration with numerical fit (straight line) using $W_{22} = 9 \times 10^{-17}$ cm$^3$/s. (Upper curve) Simulation using $W_{22}$ from the literature (see Table I, $W_{22} = 1.8 \times 10^{-17}$ cm$^3$/s).

(2–3 ms). Experimentally, 0.43 mJ were measured at a duration of 250 $\mu$s, corresponding to 1.7 W of average power.

The first phase of the output power curve as a function of time coincides with a period in which the upper laser level is already strongly populated whereas the lower laser level is not. During this period, stimulated emission and ETU $W_{22}$ dominate the temporal evolution of the lasers output. At a later moment, the lower laser level becomes populated and the ETU $W_{11}$, which depends quadratically on the population of this level, starts to dominate the laser behavior [8].This is shown in Fig. 3(c), where we used a pump pulse of 3 ms duration, and otherwise, the same parameters, as shown in Table I. The simulation in Fig. 3(c) does not include the Boltzmann factor of the laser levels and represents the total fraction of occupation.

The slope efficiency is shown in Fig. 4. Using the least-square method, a threshold of 8.7(18) W and slope efficiency of 0.119(10) were calculated. The cavity losses, calculated with Findlay–Clay analysis [9] using 3-ms-long pump pulses, are 3.9(14)% and the small signal single pass gain is 0.32(8) cm$^{-1}$ (Fig. 4).

For comparison, the highest CW output power reported so far is 1.8 W [10] obtained by using power scaling through diode-side-pumping. The highest slope efficiency reported is 50% in CW operation [11] under Ti:sapphire pumping. This high slope efficiency shows clearly the importance of energy recycling by the ETU $W_{11}$ under CW pumping. Efficiencies under qCW pumping are comparably much lower [12], [13], being close to 10%.

The atypical pulse power enhancement at pulse start has been observed before in an Er:ZBLAN fiber laser but its cause could not be explained [14]. The strong decrease of the output power at the beginning [see Fig. 3(a)] seems to be the result of a process that competes with stimulated emission. Among the main mechanism outlined in Section I, there are three processes that decrease the population of the upper laser level or the inversion itself.

1) The ESA $R_{26}$, which has a linear dependency on the upper laser level population [see (3)], is based on the absorption of two photons by the same ion, and therefore, depending on the pump condition, is of low probability, which makes this effect very week. From the numerical simulation, it was found that in steady-state operation the rate at which this process depopulates the upper laser level is negligible when compared to the ETU process $W_{22}$. Even in the absence of $W_{22}$ or if the pumping conditions were such that ESA were predominant, ESA would influence the pulse characteristics right from the start, and therefore, cause only a lower output power but no decrease as a function of pulse duration.
2) The $W_{50}$ process is a cross-relaxation originating from the $^4S_{3/2}$ energy level and from the ground level, and populating the upper and the lower laser levels. The $^4S_{3/2}$ level becomes populated by nonradiative decay from $^4F_{7/2}$ after occupation of this level by ETU $W_{22}$ and ESA $R_{26}$. The cross-relaxation $W_{50}$ is the main mechanism that depopulates the higher energy levels and has to be studied in context with $W_{22}$: whenever $W_{22}$ withdraws two electrons from the upper laser level, $W_{50}$ redistributes them to the upper and lower laser level diminishing the total inversion by two. Therefore, $W_{50}$ is of special importance during second phase of the pulse, when the ETU $W_{11}$ promotes population from the lower laser level to the upper laser level. It also matters during the first phase, because for every two electrons removed from the upper laser level by $W_{22}$, one is returned by $W_{50}$, diminishing the total occupation by one and not by two electrons. This scheme effectively works because at the high doping level of 15 mol% used in this experiment, the fluorescence lifetime of the combined $^4S_{3/2}/^2H_{11/2}$ energy level drops to less than 20 $\mu$s allowing for almost instantaneous energy recycling [9], [15].
3) The ETU $W_{22}$ is a much slower process than the ESA $R_{26}$ and it also depends quadratically on population. Both arguments are in agreement with the observed decay of the pulse output power during phase 1.

Using the parameters from Table I, our simulations did not show (upper line in Fig. 5) the temporal behavior we observed experimentally in Fig. 3(b). By the simulation, the average output power increased steadily with pulse duration until it reaches its CW condition, which is in disagreement with our experimental results (see Fig. 4) but seemed in part in agreement with the observations from [11]. Changing the value of the $W_{22}$ to $9 \times 10^{-17}$ cm$^3$/s resulted in a good fit with our results as demonstrated by the dashed line in Fig. 5.

Our simulations show that in the absence of both ETU ($W_{11}$ and $W_{22}$) a triangular laser pulse of 9.7 ms total duration occurs that steadily decreases with time. The fact that the duration of this pulse is comparable to the lower laser level lifetime demonstrates the self terminated nature of the involved laser levels. In the absence of only $W_{11}$ and using previous value for $W_{22}$ a short pulse of approximately 350 $\mu$s (duration at pulse base) is

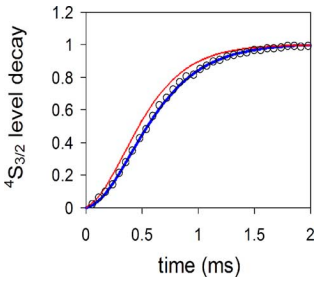


Fig. 6. Experimental measurement (normalized values) of the $^4S_{3/2}$ level emission (dots) and simulations using $W_{22} = 9 \times 10^{-17}$ cm$^3$/s (line through dots) and the value of the literature of $W_{22} = 1.8 \times 10^{-17}$ cm$^3$/s (line above dots).

obtained at the high pump intensities involved in our experiment (12 kW/cm$^2$). This pulse length is comparable to the duration of the pulses with the highest output power encountered in our experiment [see Fig. 3(b)]. Therefore, it seems that $W_{22}$ is the main responsible effect for the pulse shaping at the beginning of the laser action and also that short-pulse lasing is possible even in the absence of $W_{11}$.

## V. Laser Spectroscopy

The rate of $W_{22}$ has been calculated previously (see Table I) by measuring the 550 nm emission from the $^2S_{3/2}$ level and fitting the result with a rate-equation model whose adjustable parameters were $W_{11}$ and $W_{22}$ [9]. The same researchers have employed another method and obtained similar values using only the first temporal part of the $^4I_{11/2}$ decay curve after direct, short-pulse excitation, during which time only $W_{22}$ is presumed to be active [16], [19]. Another group determined the $W_{22}$ parameter by monitoring the 556 nm emission under 970–980 nm transient excitation and comparing with direct excitation at 540 nm [17].

In our experiment, the emission of the $^4S_{3/2}$ level at 556 nm was observed at 90° to the resonator axis with a monochromator and a photomultiplier (see Fig. 2) under 2.8 $\mu$m lasing operation using a pump power of 22 W. Fig. 6 shows the fit between the $^4S_{3/2}$ level spontaneous emission and the simulation for this mechanism, assuming $W_{22} = 9 \times 10^{-17}$ cm$^3$/s.

The higher value for the ETU $W_{22}$ is the reason why the laser decreases its output power in the first few hundreds of microseconds. When the $^4I_{11/2}$ upper laser level becomes populated, this ETU introduces a loss that increases with the square of the population of this level, competing with the stimulated emission, therefore, decreasing the output power.

The decay at the beginning of the pulse is indicative for a process that does not depend linearly on the upper laser level population. This could be verified in our simulations, which demonstrated clearly that no other process than $W_{22}$ (the only process that depends quadratically on $N_2$) is capable of reproducing the experimentally obtained pulse decay. During the simulation procedure, the other parameters were systematically changed over several magnitudes and in several combinations. The final set of parameters corresponds to the ones cited in the references of Table I, with exception of $W_{22}$.

## VI. Conclusion

An output power increase at the beginning of the pulses of a 2.8 $\mu$m, qCW diode-pumped Er:YLF laser is demonstrated for the first time. The laser generates higher average output power when operated at 250 $\mu$s pulse duration than for longer pulses. When operating in this regime 60% more efficiency is obtained than with pulses of several millisecond duration. This effect is credited to a strong pulse modulation by the ETU from the upper laser level, $W_{22}$. The experimental data for the average output power are well fitted by a value of $9 \times 10^{-17}$ cm$^3$/s for the $W_{22}$ process. Good agreement is obtained when using this value to fit the experimentally measured spontaneous green emission from $^4S_{3/2}$ energy level.

## References

[1] J. Frauchiger and W. Lüthy, "Interaction of 3 $\mu$m radiation with matter," *Opt. Quantum Electron.*, vol. 19, pp. 231–235, 1987.

[2] M. Frenz, C. Mischler, V. Romano, M. Forrer, O. M. Müller, and H. P. Weber, "Effect of mechanical tissue properties on thermal damage after IR-laser ablation," *Appl. Phys. B*, vol. 52, pp. 251–258, 1991.

[3] R. C. Stoneman, J. G. Lynn, and L. Esterowitz, "Direct upper-state pumping of the 2.8 $\mu$m Er$^{3+}$:YLF laser," *IEEE J. Quantum Electron.*, vol. 28, no. 4, pp. 1041–1045, Apr. 1992.

[4] M. Pollnau, T. Graf, J. E. Balmer, W. Lüthy, and H. P. Weber, "Explanation of the cw operation of the Er3+ 3-mm crystal laser," *Phys. Rev.A*, vol. 49, no. 5, pp. 3990–3996, 1994.

[5] K. L. Vodopyanov, A. V. E. Lukashev, and C. C. Philips, *Opt. Commun.*, vol. 95, p. 87, 1993.

[6] E. Siegman, M. W. Sasnett, and T. F. Johnston, "Choice of clip levels for beam width measurements using knife-edge techniques," *IEEE J. Quantum Electron.*, vol. 27, no. 4, pp. 1098–1104, Apr. 1991.

[7] A. M. Deana and N. U. Wetter, "1.75 W 3 $\mu$s pulsed Er:YLF laser diode end and side-pumped MOPA," in *Encontro Nacional de Física da Matéria Condensada 2007, São Lourenço/MG, Optics Technical Digest* (Sociedade Brasileira de Física), São Paulo, Brazil, 2007, pp. 173–176.

[8] W. Lupei, S. Georgescu, and V. Florea, "On the dynamics of population inversion for 3 $\mu$m Er3+ lasers," *IEEE J. Quantum Electron.*, vol. 29, no. 2, pp. 426–434, Feb. 1993.

[9] H. Chou and H. P. Jenssen, "Upconversion processes in Er-activated solid state laser materials," in *Tunable Solid State Lasers* (OSA Proceedings Series, Vol. 5), M. L. Shand and H. P. Jenssen, Eds. Washington, DC: Optical Society of America, 1989, pp. 167–174.

[10] M. Pollnau, W. Lüthy, H. P. Weber, K. Krämer, H. U. Güdel, and R. A. McFarlane, "Excited-state absorption in Er:BaY2F8 and Cs3Er2Br9 and comparison with Er:LiYF$_4$," *Appl. Phys. B*, vol. 52, pp. 339–344, 1996.

[11] M. Pollnau, R. Spring, S. Wittwer, W. Lüthy, and H. P. Weber, "Investigations on the slope efficiency of a pulsed 2.8-$\mu$m Er :LiYF laser," *J. Opt. Soc. Amer. B, Opt. Image Sci.*, vol. 14, no. 4, pp. 974–978, 1997.

[12] M. Pollnau, R. Spring, C. Ghisler, S. Wittwer, W. Lüthy, and H. P. Weber, "Efficiency of erbium 3-$\mu$m crystal and fiber lasers," *IEEE J.Quantum Electron.*, vol. 32, no. 4, pp. 657–663, Apr. 1996.

[13] D. Findlay and R. A. Clay, "The measurement of internal losses in 4-level lasers," *Phys. Lett.*, vol. 20, pp. 277–278, 1966.

[14] A. Y. Dergachev, J. H. Flint, and P. F. Moulton, "1.8-W CW Er:YLF diode-pumped laser," in *Lasers Electro-Opt., OSA Tech. Dig. (Opt. Soc. Amer.)*, Washington, DC, 2000, pp. 564–565.

[15] C. Wyss, W. Lüthy, H. P. Weber, P. Rogin, and J. Hulliger, "Emission properties of an optimized 2.8 $\mu$m Er:YLF laser," *Opt. Commun.*, vol. 139, pp. 215–218, 1997.

[16] T. Jensen, G. Huber, and K. Petermann, S. A. Payne and C. R. Pollock, Eds., "Quasi-cw diode pumped 2.8 $\mu$m laser operation of Er -doped garnets," in *OSA Proc. Adv. Solid-State Lasers*, Washington, DC, 1996, pp. 306–308.

[17] H. Voss and F. Massman, , C. R. Pollock and W. R. Bosenberg, Eds., "Diode pumped, Q-switched Erbium lasers with short pulse duration," in *Advanced Solid State Lasers* (OSA Trends in Optics and Photonics Series, Vol. 10). Washington, DC: Optical Society of America, 1997, pp. 217–221.

[18] B. C. Dickinson, P. S. Golding, M. Pollnau, T. A. King, and S. D. Jackson, "Investigation of a 791-nm pulse-pumped 2.7 $\mu$m Er doped ZBLAN fiber laser," *Opt. Commun.*, vol. 191, pp. 315–321, 2001.

[19] P. S. Golding, S. D. Jackson, T. A. King, and M. Pollnau, "Energy-transfer processes in Er -doped and Er, Pr -codoped ZBLAN glasses," *Phys. Rev. B*, vol. 62, no. 2, pp. 856–864, 2000.

[20] T. Jensen, "Upconversion-prozesse und Wirkungsquerschnitte in Er-dotierten 3 $\mu$m fluorid- und granat-lasern, gepumpt mit cw und quasi-cw dioden-arrays,," Ph.D. dissertation, Inst. Laser-Phys., Univ. Hamburg, Hamburg, Germany, 1996.

[21] A. Jagosich and F. Henrique, "Studies of the energy transfer processes from $Er^{3+}$ and $Ho^{3+}$ to $Nd^{3+}$, $Tb^{3+}$ or $Eu^{3+}$ in $LiYF_4$ crystals and ZBLAN glasses for laser media optimization operating near 3 $\mu$m region,," Ph.D, dissertation, Inst. de Pesquisas Energéticas e Nucleares, São Paulo, Brazil, 2006.

**Niklaus Ursus Wetter** received the B.Sc. degree in physics from the Federal Institute of Technology of Zürich (ETHZ), Zürich, Switzerland, in 1988, and the Ph.D. degree from the Institute of Energetic and Nuclear Research, University of São Paulo, São Paulo, Brazil, in 1993.

He is currently a Senior Researcher and the Head of laser development at the Centro de Lasers e Aplicações, IPEN-CNEN/SP, São Paulo. His current research interests include laser design, high-power, diode-pumped lasers, and nanomaterials for the enhancement of stimulated emission.

Dr. Wetter is a member of the Brazilian Physical Society and the Optical Society of America.

**Alessandro Melo Deana** received the B.Sc. degree in physics from the University of São Paulo (USP), São Paulo, Brazil, in 2003, and the Ph.D. degree from the Institute of Energetic and Nuclear Research, USP, in 2008.

He is currently a Consultant in laser development at MedCompany, São Paulo. His current research interests include laser design, high-power, diode-pumped lasers, lamp-pumped lasers, and biomedical applications of lasers.

Dr. Deana is a member of the Brazilian Physical Society.

**Izilda Marcia Ranieri** received the B.Sc. degree in physics, and the M.Sc. and Ph.D. degrees in nuclear technology applications from the University of São Paulo (USP), São Paulo, Brazil, 1976, 1979, and 2001, respectively.

Since 1979, she has been with the Instituto de Pesquisas Energéticas e Nucleares, Centro de Lasers e Aplicações, CNEN-IPEN/SP, São Paulo, where she is currently a Senior Researcher. Her current research interests include synthesis, purification, and crystal growth of fluorides, and phase diagram construction.

**Laércio Gomes** was born in Brazil on April 2, 1950. He received the Ph.D. degree from the University of São Paulo, São Paulo, Brazil, in 1985.

He was engaged in research of comprehensive study of $OH^-$ photodissociation in alkali halides crystals and the luminescence quenching effects of F centers correlated to the $OH^-$ molecular ions, and was engaged in the investigation of the mechanism of nonradiative energy transfer between trivalent rare earth ions in solids. Since 1990, he has been with the Centro de Lasers e Aplicações, IPEN-CNEN/SP, where he is involved in rare-earth-doped fluoride and glasses to develop new laser materials.

**Sonia Licia Baldochi** received the B.Sc. degree in physics from Pontifical Catholic University, São Paulo, Brazil, 1981, and the M.Sc. and Ph.D. degrees in nuclear technology–materials area from São Paulo University, São Paulo, in 1985 and 1993, respectively.

In 1998, she was a Postdoctoral Researcher with the Institute for Materials Research, Tohoku University, Tohoku, Japan. In 1985, she has joined Nuclear and Energy Research Institute, IPEN, where she has been with the Crystal Growth Group since 1999, and in charge of the Materials and Laser Technology Division from 2000 to 2007. Since 2008, she has been the Manager of the Center for Lasers and Applications, IPEN-CNEN/SP, where she is currently a Senior Research Fellow. Her current research interests include synthesis and crystal growth of bulk fluorides crystals, and fluoride and oxides single crystal fibers for optical applications.